

Unified neural output-constrained control for space manipulator using tan-type barrier Lyapunov function

Hadi Jahanshahi^{a,*}, Qijia Yao^b, Muhammad Ijaz Khan^c, Irene Moroz^d

a. Department of Mechanical Engineering, University of Manitoba, Winnipeg R3T 5V6, Canada

b. School of Aerospace Engineering, Beijing Institute of Technology, Beijing 100081, China

c. Department of Mechanical Engineering, Lebanese American University, Beirut, Lebanon

d. Mathematical Institute, University of Oxford, Oxford, OX2 6GG, England, UK

Abstract

In this paper, a unified neural control scheme is presented for the output-constrained trajectory tracking of space manipulator under unknown parameters and external perturbations. By utilizing the backstepping control technique as the main framework, the proposed controller is developed with the help of neural network (NN) and tan-type barrier Lyapunov function (BLF). The NN is introduced to identify the unknown part in the dynamic model of the space manipulator. Benefiting from the neural identification, the proposed controller is model-free and insensitive to external perturbations. Moreover, the BLF is adopted to guarantee the position tracking errors never exceed the predefined output constraints. Different from log-type BLF, the tan-type BLF is employed for the control design, which makes the proposed controller universal for the cases with and without considering the output constraints. The semiglobal uniform ultimate boundedness of the resulting closed-loop system is strictly obtained through stability argument. All error variables in the closed-loop system can eventually stabilize to the small residual sets about zero under the proposed controller. Lastly, simulations and comparisons are given to demonstrate the effectiveness and excellent tracking performance of the proposed control scheme.

Keywords: Space manipulator; Trajectory tracking control; Output constraints; Neural identification; Tan-type barrier Lyapunov function

* Corresponding author

1. Introduction

Nowadays, the space manipulator has played an important role in a variety of space missions, such as on-orbit servicing, large space structure assembly, and active debris removal. Generally, the space manipulator is composed of a spacecraft base and one or more manipulators mounted on it. The dynamic model of the space manipulator is highly nonlinear and strongly coupled. Any motion of the manipulator links can have a great effect on the motion of the spacecraft base and vice versa. Meanwhile, due to the complex space environment, the space manipulator unavoidably suffers from uncertain parameters and external perturbations. Even worse, when the space manipulator is utilized for the non-cooperative target capturing, the model information of the space target may be fully unknown in advance. As a result, the above issues bring a great difficulty to the space manipulator control system design.

Depending on whether the spacecraft base is controllable, the working modes of the space manipulator can be divided into the free-floating mode and free-flying mode. The free-flying mode can be further divided into the fully free-flying mode and attitude-controlled free-flying mode (Moosavian and Papadopoulos, 2007). When the space manipulator captures a non-cooperative target, it usually works in the attitude-controlled free-flying mode. On the one hand, the space manipulator can accomplish the target capturing with a relatively simple configuration. On the other hand, the possible collision danger can be avoided since the spacecraft base is floating and its position is not in control. During the past decades, with the rapid development of space robotic technology, many space demonstration experiments have been made by aerospace powers, such as Space Robot Technology Experiment (ROTEX) by Germany in 1993, Engineering Test Satellite-VII (ETS-VII) by Japan in 1997, and Orbital Express (OE) by the US in 2007 (Flores-Abad et al., 2014; Li et al., 2019; Moghaddam and Chhabra, 2021).

Until recently, a large range of advanced control algorithms have been employed for the trajectory tracking control of space manipulator. Parlaktuna and Ozkan (2004) presented an adaptive computed-torque control method for a free-floating space manipulator based on the dynamically equivalent manipulator model. In Wang (2011) and Wang and Xie (2009a; 2009b; 2012), several adaptive tracking controllers were developed for a free-floating space manipulator by utilizing adaptive inverse dynamics, prediction error based adaptation, and passivity based adaptation, respectively. Chu et al. (2015) presented a composite hierarchical control strategy for a space manipulator based on the improved sliding mode control and an uncertainty and disturbance estimator. In Yu and Chen (2015), an observer-based augmented adaptive controller was designed for a flexible-joint space manipulator by introducing the singular perturbation theory. Yang et al. (2015) developed a nonlinear decoupling feedback

control scheme for the trajectory tracking of a two-link flexible manipulator based on the backstepping control method and an extended state observer. In [Jayakody et al. \(2016\)](#), an adaptive variable structure control method was applied to design a robust coordination controller for a free-flying space robot subject to system uncertainties. [Rybus et al. \(2017\)](#) constructed a new control system for a free-floating space manipulator which is composed of an optimal trajectory planning module and a nonlinear model predictive controller. In [Shi et al. \(2017\)](#), a sliding mode controller and a nonlinear model predictive controller were developed for the robust coordinated control of a dual-arm space robot under system uncertainties. [Jia et al. \(2018\)](#) presented a composite control strategy for the maneuver and vibration suppression of a free-flying flexible space robot actuated by control moment gyros. In [Nekoo \(2019\)](#), a model reference adaptive control approach was employed for the regulation and tracking of a free-floating space manipulator based on the state-dependent Riccati equation. [Seddaoui and Saaj \(2019\)](#) designed a combined nonlinear H_∞ controller for a controlled-floating space robot subject to internal uncertainties and environmental perturbations. [Shao et al. \(2021\)](#) proposed a nonsingular terminal sliding mode control scheme for a free-floating space manipulator in the presence of disturbances. In [Jin et al. \(2021\)](#), a fixed-time position and attitude control method was developed for a space robot in task space based on an extended state observer. [Yao \(2022\)](#) presented a robust finite-time tracking control method for a free-flying space manipulator by integrating with a disturbance observer.

Although the above control methods have the strong robustness against uncertain parameters and external perturbations, most of them are designed based on the nominal dynamic model of the space manipulator. When the model information of the space manipulator is fully unknown, these controllers are no longer applicable. It is well recognized that the neural network (NN) and fuzzy logic system have the powerful global identification capability ([Zhang et al., 2021a, 2021b, 2022](#)). The intelligent control is an effective approach to handle the unknown parameters and external perturbations by introducing NN or fuzzy logic system to identify the unknown part in the dynamic model of the space manipulator. [Pazelli et al. \(2011\)](#) proposed several robust H_∞ control methods for a free-floating space manipulator based on the NN and fuzzy logic system, respectively. In [Kumar et al. \(2013\)](#), an adaptive NN-based controller was developed for a space robot system with an attitude controlled base. [Zhang et al. \(2013\)](#) presented a model-free output feedback control strategy was carried out for a free-floating space manipulator based on the adaptive fuzzy NN. In [Chu et al. \(2014\)](#), an adaptive fuzzy output control scheme was proposed for the robust tracking of a space manipulator based on a disturbance observer. [Qin et al. \(2014\)](#) designed a fuzzy adaptive

robust controller for a space robot considering the effect of gravity. [Jia and Shan \(2020\)](#) developed a NN-based adaptive terminal sliding mode controller for the finite-time trajectory tracking of space manipulator under actuator saturation. In [Jia et al. \(2021\)](#), an adaptive fuzzy terminal sliding mode control method was presented for a free-floating space manipulator with free-swinging joint failures. [Zhan et al. \(2022\)](#) proposed an extended state observer-based adaptive controller for a flexible-joint space manipulator by adopting NN to compensate the system uncertainties.

Besides, the output constrained control is another hot research topic for the trajectory tracking of space manipulator to ensure safety. The prescribed performance control is a commonly used approach to deal with the output constraints by the aid of coordinate transformation. [Zhou et al. \(2017\)](#) designed a prescribed performance robust tracking controller for a free-floating space manipulator with kinematic and dynamic uncertainties. [Zhu et al. \(2019\)](#) implemented an adaptive disturbance observer-based composite control approach to a space manipulator for target capturing with prescribed performance. The barrier Lyapunov function (BLF) is another effective tool to handle the output constraints. The BLF is a special class of Lyapunov function which grows to infinity when the system outputs approach the certain bounds. In this way, the BLF-based control can preserve the system outputs always within the predefined output constraints. Generally, the BLF can be classified into the log-type BLF ([Tee et al., 2009, 2011](#); [Ren et al., 2010](#)) and tan-type BLF ([Jin and Xu, 2013](#); [Xu and Jin, 2013](#)). [Yao \(2021a\)](#) developed a neural adaptive state feedback controller and a neural adaptive output feedback controller for the trajectory tracking of a space manipulator with output constraints. The similar neural adaptive state feedback controller was also applied in [Yao \(2021b\)](#). Particularly, the input nonlinearities were taken into account therein. However, the above controllers were mainly designed based on the log-type BLF. To the best of the authors' knowledge, the tan-type BLF has been never utilized for the space manipulator control system design.

The above observations motivate our study. In this paper, the challenging problem of the output-constrained trajectory tracking of space manipulator under unknown parameters and external perturbations is investigated. A unified neural control scheme is originally proposed to solve this problem. By utilizing the backstepping control technique as the main framework, the proposed controller is developed with the help of NN and tan-type BLF. The main contributions of this research can be summarized as the following three aspects.

- The NN is introduced to identify the unknown part in the dynamic model of the space manipulator. Benefiting from the neural identification, the proposed controller is model-free and insensitive to external perturbations.

• The BLF is adopted to guarantee the position tracking errors never exceed the predefined output constraints. Different from log-type BLF, the tan-type BLF is employed for the control design, which makes the proposed controller universal for the cases with and without considering the output constraints.

• The semiglobal uniform ultimate boundedness of the resulting closed-loop system is strictly obtained through stability argument. All error variables in the closed-loop system can eventually stabilize to the small residual sets about zero under the proposed controller.

The rest of this paper is arranged as follows. Section 2 describes the problem and presents some preliminaries. Section 3 provides the control design and stability argument. Section 4 gives the simulations and comparisons. Lastly, Section 5 concludes this work.

2. Problem description and preliminaries

2.1. Dynamics of the space manipulator

Suppose an attitude-controlled free-flying space manipulator composed of a spacecraft base B_0 and a manipulator with n links B_i ($i = 1, 2, \dots, n$) as depicted in Fig. 1. C_i denotes the joint center between B_{i-1} and B_i . O_i denotes the mass center of B_i . O_c denotes the mass center of the whole space manipulator system. m_i and I_i are the mass and moment of inertia of B_i , respectively. Construct the initial reference frame $OXYZ$ with the center fixed at O and the body-fixed frame $O_iX_iY_iZ_i$ ($i = 0, 1, \dots, n$) with the center fixed at O_i .

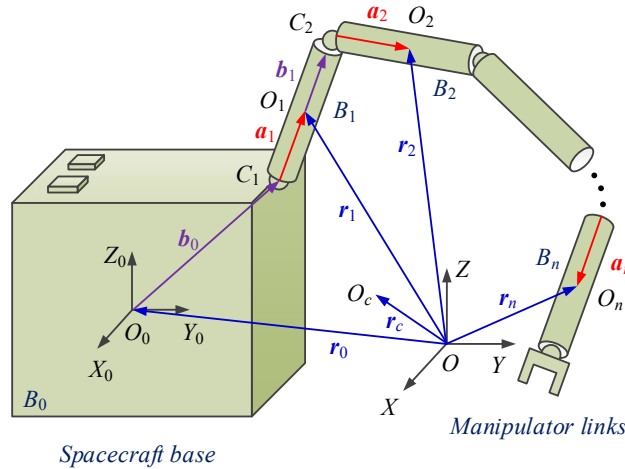


Fig. 1. General model of an attitude-controlled free-flying space manipulator.

According to the geometric relations in Fig. 1, the position vector from O to O_i can be expressed as

$$\mathbf{r}_i = \mathbf{r}_0 + \mathbf{b}_0 + \sum_{j=1}^{i-1} (\mathbf{a}_j + \mathbf{b}_j) + \mathbf{a}_i, \quad (1)$$

where \mathbf{a}_i ($i=1,2,\dots,n$) is the position vector from C_i to O_i and \mathbf{b}_i ($i=0,1,\dots,n-1$) is the position vector from O_i to C_{i+1} . The velocity of B_i can be expressed as

$$\begin{aligned} \mathbf{v}_i &= \mathbf{v}_0 + \boldsymbol{\omega}_0 \times (\mathbf{r}_i - \mathbf{r}_0) + \sum_{j=1}^i (\mathbf{z}_j \times (\mathbf{r}_i - \mathbf{r}_j)) \dot{q}_j \\ &= \begin{bmatrix} \mathbf{I}_3 & \mathbf{r}_{i0}^\times \end{bmatrix} \begin{bmatrix} \mathbf{v}_0 \\ \boldsymbol{\omega}_0 \end{bmatrix} + \mathbf{J}_{vi} \dot{\mathbf{q}}_m, \end{aligned} \quad (2)$$

where \mathbf{z}_i is the unit vector along the joint C_i , q_i is the rotation angle of B_i , $\mathbf{q}_m = [q_1, q_2, \dots, q_n]^\top$, $\mathbf{r}_{i0} = \mathbf{r}_0 - \mathbf{r}_i$, $\mathbf{J}_{vi} = [\mathbf{z}_1 \times (\boldsymbol{\rho}_i - \mathbf{p}_1) \quad \mathbf{z}_2 \times (\boldsymbol{\rho}_i - \mathbf{p}_2) \quad \dots \quad \mathbf{z}_j \times (\boldsymbol{\rho}_i - \mathbf{p}_j) \quad \mathbf{0}_3 \quad \dots \quad \mathbf{0}_3]$, and the symbol $(\cdot)^\times$ is defined as the skew-symmetric operator of a vector. Moreover, the angular velocity of B_i can be expressed as

$$\begin{aligned} \boldsymbol{\omega}_i &= \boldsymbol{\omega}_0 + \sum_{j=1}^i \mathbf{z}_j \dot{q}_j \\ &= \boldsymbol{\omega}_0 + \mathbf{J}_{oi} \dot{\mathbf{q}}_m, \end{aligned} \quad (3)$$

where $\mathbf{J}_{oi} = [\mathbf{z}_1 \quad \mathbf{z}_2 \quad \dots \quad \mathbf{z}_i \quad \mathbf{0}_3 \quad \dots \quad \mathbf{0}_3]$. For a free-flying space manipulator, the total linear momentum is conserved since there are no external forces acted on it. Without loss of generality, the initial linear momentum of the space manipulator is assumed to be zero. The total linear momentum of the space manipulator can be expressed as

$$\begin{aligned} \mathbf{P} &= \sum_{i=0}^n m_i \mathbf{v}_i \\ &= \sum_{i=0}^n \left(m_i \begin{bmatrix} \mathbf{I}_3 & \mathbf{r}_{i0}^\times \end{bmatrix} \begin{bmatrix} \mathbf{v}_0 \\ \boldsymbol{\omega}_0 \end{bmatrix} + m_i \mathbf{J}_{vi} \dot{\mathbf{q}}_m \right) \\ &= \begin{bmatrix} m_c \mathbf{I}_3 & m_c \mathbf{r}_{c0}^\times \end{bmatrix} \begin{bmatrix} \mathbf{v}_0 \\ \boldsymbol{\omega}_0 \end{bmatrix} + \mathbf{J}_{mv} \dot{\mathbf{q}}_m \\ &= \mathbf{0}_3, \end{aligned} \quad (4)$$

where $m_c = \sum_{i=0}^n m_i$, $\mathbf{r}_{c0} = \mathbf{r}_0 - \mathbf{r}_c$, and $\mathbf{J}_{mv} = \sum_{i=0}^n m_i \mathbf{J}_{vi}$. Rearranging (4), we can obtain

$$\mathbf{v}_0 = -\mathbf{r}_{c0}^\times \boldsymbol{\omega}_0 - m_c^{-1} \mathbf{J}_{mv} \dot{\mathbf{q}}_m. \quad (5)$$

On the other hand, the total kinetic energy of the space manipulator can be expressed as

$$T = \frac{1}{2} \sum_{i=0}^n (\omega_i^T I_i \omega_i + m_i \mathbf{v}_i^T \mathbf{v}_i). \quad (6)$$

Substituting (2), (3), and (5) into (6) and rearranging it, we eventually have

$$\begin{aligned} T &= \frac{1}{2} \begin{bmatrix} \omega_0^T & \dot{\mathbf{q}}_m^T \end{bmatrix} \begin{bmatrix} \mathbf{H}_b & \mathbf{H}_{bm} \\ * & \mathbf{H}_m \end{bmatrix} \begin{bmatrix} \omega_0 \\ \dot{\mathbf{q}}_m \end{bmatrix} \\ &= \frac{1}{2} \dot{\mathbf{q}}^T \mathbf{H}(\mathbf{q}) \dot{\mathbf{q}}, \end{aligned} \quad (7)$$

where the matrices \mathbf{H}_b , \mathbf{H}_{bm} , and \mathbf{H}_m are defined as

$$\mathbf{H}_b = \sum_{i=0}^n (I_i + m_i \mathbf{r}_{i0}^{\times T} \mathbf{r}_{i0}^{\times}) - m_c \mathbf{r}_{c0}^{\times T} \mathbf{r}_{c0}^{\times}, \quad (8)$$

$$\mathbf{H}_{bm} = \sum_{i=1}^n (I_i \mathbf{J}_{\omega i} + m_i \mathbf{r}_{i0}^{\times T} \mathbf{J}_{vi}) - \mathbf{r}_{c0}^{\times T} \mathbf{J}_{mv}, \quad (9)$$

$$\mathbf{H}_m = \sum_{i=1}^n (\mathbf{J}_{\omega i}^T I_i \mathbf{J}_{\omega i} + m_i \mathbf{J}_{vi}^T \mathbf{J}_{vi}) - \frac{\mathbf{J}_{mv}^T \mathbf{J}_{mv}}{m_c}. \quad (10)$$

Since the space manipulator works in the micro-gravity environment, the potential energy of the space manipulator can be neglected. The total energy of the space manipulator is its total kinetic energy. The Lagrangian equation is provided as

$$\frac{d}{dt} \left\{ \frac{\partial T}{\partial \dot{\mathbf{q}}} \right\} - \frac{\partial T}{\partial \mathbf{q}} = \mathbf{Q}, \quad (11)$$

where \mathbf{Q} represents the generalized forces. Substituting (7) into (11), the dynamic model of the space manipulator can be described as

$$\mathbf{H}(\mathbf{q}) \ddot{\mathbf{q}} + \mathbf{C}(\mathbf{q}, \dot{\mathbf{q}}) \dot{\mathbf{q}} = \boldsymbol{\tau} + \boldsymbol{\delta}, \quad (12)$$

where $\mathbf{q} = [\mathbf{q}_0^T, \mathbf{q}_m^T]^T \in \sim^l$ and $\dot{\mathbf{q}} = [\omega_0^T, \dot{\mathbf{q}}_m^T]^T \in \sim^l$ are the generalized position and velocity of the space manipulator. l denotes the total degree-of freedom (DOF) of the space manipulator. For planar case, $l = n + 1$, and for spatial case, $l = n + 3$. $\mathbf{H}(\mathbf{q}) \in \sim^{l \times l}$ is the inertia matrix, $\mathbf{C}(\mathbf{q}, \dot{\mathbf{q}}) \in \sim^{l \times l}$ is the Coriolis and centrifugal matrix, $\boldsymbol{\tau} \in \sim^l$ and $\boldsymbol{\delta} \in \sim^l$ are the control torques and external perturbations, respectively. The matrices $\mathbf{H}(\mathbf{q})$ and $\mathbf{C}(\mathbf{q}, \dot{\mathbf{q}})$ are assumed to be fully unknown in the control design. Moreover, due to the physical limitations of the practical actuators, the control torques are saturated with

$$\tau_i = \begin{cases} \tau_m, & \tau_{ci} \geq \tau_m, \\ \tau_{ci}, & -\tau_m \leq \tau_{ci} < \tau_m, \\ -\tau_m, & \tau_{ci} < -\tau_m, \end{cases} \quad (13)$$

where $\tau_c \in \sim^l$ is the command control inputs and τ_m is the maximum acceptable control torque value. Then, the saturated control torques can be rewritten as

$$\tau = \tau_c + \tau_\Delta, \quad (14)$$

where $\tau_\Delta = \tau - \tau_c$ denotes the control deviations. Subsequently, the dynamic model of the space manipulator can be rearranged as

$$H(q)\ddot{q} + C(q, \dot{q})\dot{q} = \tau_c + \tau_\Delta + \delta. \quad (15)$$

Note that system (15) has the following fundamental properties (Spong et al., 2006).

Property 1. The inertia matrix $H(q)$ is symmetric and positive definite.

Property 2. The matrix $\dot{H}(q) - 2C(q, \dot{q})$ is skew symmetric.

Property 3. The matrices $H(q)$ and $C(q, \dot{q})$ are bounded with $\underline{h}\mathbf{I}_l \leq H(q) \leq \bar{h}\mathbf{I}_l$ and $\|C(q, \dot{q})\| \leq \bar{c}\|\dot{q}\|$,

where \underline{h} , \bar{h} , and \bar{c} are positive constants.

2.2. Main objective

Define q_d as the desired position of the space manipulator and then the position and velocity tracking errors can be expressed as $q_e = q - q_d$ and $\dot{q}_e = \dot{q} - \dot{q}_d$, respectively. To ensure safety, the main objective of this work is designing an appropriate controller τ_c for the space manipulator to guarantee the position tracking errors always within the following output constraints:

$$-k_b(t) \leq q_e(t) \leq k_b(t), \quad (16)$$

where $k_b(t) = [k_{b1}(t), k_{b2}(t), \dots, k_{bl}(t)]^T \in \sim^l$ with $k_{bi}(t) > 0$ ($i = 1, 2, \dots, l$) is the predefined upper bounds.

Obviously, the initial position of the space manipulator should satisfy the condition that $-k_b(0) \leq q_e(0) \leq k_b(0)$.

2.3. NN identification

Lemma 1. (Sanner and Slotine, 1992) For a continuous nonlinear function $f(Z)$, $Z \in \sim^p$, it can be identified by a radial basis function NN (RBFNN) as

$$f(\mathbf{Z}) = \mathbf{W}^{*T} \boldsymbol{\theta}(\mathbf{Z}) + \varepsilon(\mathbf{Z}), \quad (17)$$

where $\mathbf{W}^* \in \mathbb{R}^{N \times 1}$ is the ideal NN weight, $\boldsymbol{\theta}(\mathbf{Z}) = [\theta_1(\mathbf{Z}), \theta_2(\mathbf{Z}), \dots, \theta_N(\mathbf{Z})]^T \in \mathbb{R}^N$ is the basis function vector,

$\varepsilon(\mathbf{Z})$ is the identification error bounded with $|\varepsilon(\mathbf{Z})| \leq \bar{\varepsilon}$, $\bar{\varepsilon} > 0$, and N is the neuron number. Moreover,

$\theta_i(\mathbf{Z})$ is usually chosen as the Gaussian function:

$$\theta_i(\mathbf{Z}) = \exp\left(-\|\mathbf{Z} - \boldsymbol{\Psi}_i\|^2 / b_i^2\right), \quad i = 1, 2, \dots, N, \quad (18)$$

where $\boldsymbol{\Psi}_i = [\psi_{i1}, \psi_{i2}, \dots, \psi_{ip}]^T \in \mathbb{R}^p$ is the center of $\theta_i(\mathbf{Z})$ and b_i is the width.

3. Control design and stability argument

3.1. Control design

The proposed controller is designed by utilizing the backstepping control technique as the main framework. To begin with, define the following error variables:

$$\mathbf{x}_1 = \mathbf{q}_e, \quad \mathbf{x}_2 = \dot{\mathbf{q}}_e - \boldsymbol{\alpha}, \quad (19)$$

where $\boldsymbol{\alpha} \in \mathbb{R}^l$ is the virtual stabilizer designed in the sequel. Let us consider the following tan-type BLF:

$$V_1 = \sum_{i=1}^l \frac{k_{bi}^2}{\pi} \tan\left(\frac{\pi x_{1i}^2}{2k_{bi}^2}\right). \quad (20)$$

Calculating the time differentiation of V_1 , we have

$$\begin{aligned} \dot{V}_1 &= \sum_{i=1}^l \left[\frac{x_{1i} \dot{x}_{1i}}{\cos^2\left(\frac{\pi x_{1i}^2}{2k_{bi}^2}\right)} + \frac{2k_{bi} \dot{k}_{bi}}{\pi} \tan\left(\frac{\pi x_{1i}^2}{2k_{bi}^2}\right) - \left(\frac{\dot{k}_{bi}}{k_{bi}}\right) \frac{x_{1i}^2}{\cos^2\left(\frac{\pi x_{1i}^2}{2k_{bi}^2}\right)} \right] \\ &= \sum_{i=1}^l \left[\frac{x_{1i} (x_{2i} + \alpha_i)}{\cos^2\left(\frac{\pi x_{1i}^2}{2k_{bi}^2}\right)} + \frac{2k_{bi} \dot{k}_{bi}}{\pi} \tan\left(\frac{\pi x_{1i}^2}{2k_{bi}^2}\right) - \left(\frac{\dot{k}_{bi}}{k_{bi}}\right) \frac{x_{1i}^2}{\cos^2\left(\frac{\pi x_{1i}^2}{2k_{bi}^2}\right)} \right]. \end{aligned} \quad (21)$$

Thus, the virtual stabilizer is designed as

$$\alpha = \begin{bmatrix} -\frac{k_1 k_{b1}^2}{\pi x_{11}} \sin\left(\frac{\pi x_{11}^2}{2k_{b1}^2}\right) \cos\left(\frac{\pi x_{11}^2}{2k_{b1}^2}\right) - \frac{2k_{b1} \dot{k}_{b1}}{\pi x_{11}} \sin\left(\frac{\pi x_{11}^2}{2k_{b1}^2}\right) \cos\left(\frac{\pi x_{11}^2}{2k_{b1}^2}\right) + \left(\frac{\dot{k}_{b1}}{k_{b1}}\right) x_{11} \\ -\frac{k_1 k_{b2}^2}{\pi x_{12}} \sin\left(\frac{\pi x_{12}^2}{2k_{b2}^2}\right) \cos\left(\frac{\pi x_{12}^2}{2k_{b2}^2}\right) - \frac{2k_{b2} \dot{k}_{b2}}{\pi x_{12}} \sin\left(\frac{\pi x_{12}^2}{2k_{b2}^2}\right) \cos\left(\frac{\pi x_{12}^2}{2k_{b2}^2}\right) + \left(\frac{\dot{k}_{b2}}{k_{b2}}\right) x_{12} \\ \vdots \\ -\frac{k_1 k_{bl}^2}{\pi x_{1l}} \sin\left(\frac{\pi x_{1l}^2}{2k_{bl}^2}\right) \cos\left(\frac{\pi x_{1l}^2}{2k_{bl}^2}\right) - \frac{2k_{bl} \dot{k}_{bl}}{\pi x_{1l}} \sin\left(\frac{\pi x_{1l}^2}{2k_{bl}^2}\right) \cos\left(\frac{\pi x_{1l}^2}{2k_{bl}^2}\right) + \left(\frac{\dot{k}_{bl}}{k_{bl}}\right) x_{1l} \end{bmatrix}, \quad (22)$$

where $k_i > 0$. Substituting the virtual stabilizer (22) into (21), we have

$$\dot{V}_1 = -\sum_{i=1}^l \frac{k_1 k_{bi}^2}{\pi} \tan\left(\frac{\pi x_{1i}^2}{2k_{bi}^2}\right) + \sum_{i=1}^l \frac{x_{1i} x_{2i}}{\cos^2\left(\frac{\pi x_{1i}^2}{2k_{bi}^2}\right)}. \quad (23)$$

Then, consider another Lyapunov function:

$$V_2 = V_1 + \frac{1}{2} \mathbf{x}_2^T \mathbf{H}(\mathbf{q}) \mathbf{x}_2. \quad (24)$$

Calculating the time differentiation of V_2 with the help of Property 2, we have

$$\begin{aligned} \dot{V}_2 &= \dot{V}_1 + \frac{1}{2} \mathbf{x}_2^T \dot{\mathbf{H}}(\mathbf{q}) \mathbf{x}_2 + \mathbf{x}_2^T \mathbf{H}(\mathbf{q}) \dot{\mathbf{x}}_2 \\ &= \dot{V}_1 + \mathbf{x}_2^T (-\mathbf{H}(\mathbf{q}) \dot{\alpha} - \mathbf{H}(\mathbf{q}) \ddot{\mathbf{q}}_d - \mathbf{C}(\mathbf{q}, \dot{\mathbf{q}}) \alpha - \mathbf{C}(\mathbf{q}, \dot{\mathbf{q}}) \dot{\mathbf{q}}_d + \boldsymbol{\tau}_c + \boldsymbol{\tau}_\Delta + \boldsymbol{\delta}) \\ &= \dot{V}_1 + \mathbf{x}_2^T (\boldsymbol{\tau}_c + \mathbf{N}), \end{aligned} \quad (25)$$

where \mathbf{N} is the unknown nonlinear item, denoted as

$$\mathbf{N} = -\mathbf{H}(\mathbf{q}) \dot{\alpha} - \mathbf{H}(\mathbf{q}) \ddot{\mathbf{q}}_d - \mathbf{C}(\mathbf{q}, \dot{\mathbf{q}}) \alpha - \mathbf{C}(\mathbf{q}, \dot{\mathbf{q}}) \dot{\mathbf{q}}_d + \boldsymbol{\tau}_\Delta + \boldsymbol{\delta}. \quad (26)$$

Substituting (23) into (25), we further have

$$\dot{V}_2 = -\sum_{i=1}^l \frac{k_1 k_{bi}^2}{\pi} \tan\left(\frac{\pi x_{1i}^2}{2k_{bi}^2}\right) + \sum_{i=1}^l \frac{x_{1i} x_{2i}}{\cos^2\left(\frac{\pi x_{1i}^2}{2k_{bi}^2}\right)} + \mathbf{x}_2^T (\boldsymbol{\tau}_c + \mathbf{N}). \quad (27)$$

In what follows, the RBFNN is introduced to identify the unknown nonlinear item \mathbf{N} . Define the variable

$\mathbf{Z} = [\mathbf{q}^T, \dot{\mathbf{q}}^T, \boldsymbol{\tau}_c^T]^T$. By Lemma 1, the unknown nonlinear item can be expressed as

$$\mathbf{N} = \mathbf{W}^{*T} \boldsymbol{\Theta}(\mathbf{Z}) + \boldsymbol{\varepsilon}(\mathbf{Z}), \quad (28)$$

where $\mathbf{W}^* \in \mathbb{R}^{N \times 1}$ is the ideal NN weight, $\boldsymbol{\theta}(\mathbf{Z}) \in \mathbb{R}^N$ is the basis function vector, $\boldsymbol{\varepsilon}(\mathbf{Z}) \in \mathbb{R}^1$ is the identification error bounded with $\|\boldsymbol{\varepsilon}(\mathbf{Z})\| \leq \bar{\varepsilon}$, $\bar{\varepsilon} > 0$, and N is the neuron number. Let $\hat{\mathbf{W}}$ be identification of the ideal NN weight \mathbf{W}^* . Accordingly, the unknown nonlinear item can be identified as

$$\hat{\mathbf{N}} = \hat{\mathbf{W}}^T \boldsymbol{\theta}(\mathbf{Z}). \quad (29)$$

Thus, the unified neural controller is designed as

$$\boldsymbol{\tau}_c = \begin{bmatrix} -\frac{x_{11}}{\cos^2\left(\frac{\pi x_{11}^2}{2k_{b1}^2}\right)} \\ -\frac{x_{12}}{\cos^2\left(\frac{\pi x_{12}^2}{2k_{b2}^2}\right)} \\ \vdots \\ -\frac{x_{1l}}{\cos^2\left(\frac{\pi x_{1l}^2}{2k_{bl}^2}\right)} \end{bmatrix} - k_2 \mathbf{x}_2 - \hat{\mathbf{W}}^T \boldsymbol{\theta}(\mathbf{Z}), \quad (30)$$

where $k_2 > 0$. Moreover, the NN weight learning law is given as

$$\dot{\hat{\mathbf{W}}}_i = \boldsymbol{\Gamma}_i \boldsymbol{\theta}_i(\mathbf{Z}) x_{2i} - \eta_i \boldsymbol{\Gamma}_i \hat{\mathbf{W}}_i, \quad i = 1, 2, \dots, l, \quad (31)$$

where $\boldsymbol{\Gamma}_i \in \mathbb{R}^{N \times N}$ is a positive definite matrix and η_i is a small positive constant.

3.2. Stability argument

Theorem 1. Suppose a free-flying space manipulator system under unknown parameters and external perturbations. If the unified neural controller (30) and the NN weight learning law (31) are implemented, then the resulting closed-loop system is semiglobally uniformly ultimately bounded and error variables \mathbf{x}_1 , \mathbf{x}_2 , and $\tilde{\mathbf{W}}$ can eventually stabilize to the following small residual sets about zero:

$$\boldsymbol{\Omega}_1 = \left\{ \mathbf{x}_1 \in \mathbb{R}^l \left| |x_{1i}| \leq \frac{2k_{bi}^2}{\pi} \tan^{-1}\left(\frac{\pi\mu}{k_{bi}^2}\right), \quad i = 1, 2, \dots, l \right. \right\}, \quad (32)$$

$$\boldsymbol{\Omega}_2 = \left\{ \mathbf{x}_2 \in \mathbb{R}^l \left| \|\mathbf{x}_2\| \leq \sqrt{\frac{2\mu}{\lambda_{\min}(\mathbf{H}(\mathbf{q}))}} \right. \right\}, \quad (33)$$

$$\boldsymbol{\Omega}_3 = \left\{ \tilde{\mathbf{W}} \in \mathbb{R}^{N \times l} \left| \|\tilde{\mathbf{W}}_i\| \leq \sqrt{\frac{2\mu}{\lambda_{\min}(\boldsymbol{\Gamma}_i^{-1})}}, \quad i = 1, 2, \dots, l \right. \right\}, \quad (34)$$

where $\mu > 0$ is defined in the sequel and the symbols $\lambda_{\min}(\cdot)$ and $\lambda_{\max}(\cdot)$ represent the minimum and maximum eigenvalues of a matrix, respectively.

Proof. Let us consider the following Lyapunov function:

$$V_3 = V_2 + \frac{1}{2} \sum_{i=1}^l \tilde{\mathbf{W}}_i^T \boldsymbol{\Gamma}_i^{-1} \tilde{\mathbf{W}}_i, \quad (35)$$

where $\tilde{\mathbf{W}} = \hat{\mathbf{W}} - \mathbf{W}^*$ denotes the identification error of \mathbf{W}^* . Calculating the time differentiation of V_3 and Substituting (27) into it, we have

$$\begin{aligned} \dot{V}_3 &= \dot{V}_2 + \sum_{i=1}^l \tilde{\mathbf{W}}_i^T \boldsymbol{\Gamma}_i^{-1} \dot{\tilde{\mathbf{W}}}_i \\ &= -\sum_{i=1}^l \frac{k_1 k_{bi}^2}{\pi} \tan\left(\frac{\pi x_{1i}^2}{2k_{bi}^2}\right) + \sum_{i=1}^l \frac{x_{1i} x_{2i}}{\cos^2\left(\frac{\pi x_{1i}^2}{2k_{bi}^2}\right)} + \mathbf{x}_2^T (\boldsymbol{\tau}_c + \mathbf{N}) + \sum_{i=1}^l \tilde{\mathbf{W}}_i^T \boldsymbol{\Gamma}_i^{-1} \dot{\tilde{\mathbf{W}}}_i. \end{aligned} \quad (36)$$

Substituting the unified neural controller (30) and the NN weight learning law (31) into (36), we have

$$\begin{aligned} \dot{V}_3 &= -\sum_{i=1}^l \frac{k_1 k_{bi}^2}{\pi} \tan\left(\frac{\pi x_{1i}^2}{2k_{bi}^2}\right) + \mathbf{x}_2^T (-k_2 \mathbf{x}_2 - \hat{\mathbf{W}}^T \boldsymbol{\Theta}(\mathbf{Z}) + \mathbf{W}^{*T} \boldsymbol{\Theta}(\mathbf{Z}) + \boldsymbol{\varepsilon}(\mathbf{Z})) \\ &\quad + \sum_{i=1}^l \tilde{\mathbf{W}}_i^T \boldsymbol{\Theta}_i(\mathbf{Z}) x_{2i} - \sum_{i=1}^l \eta_i \tilde{\mathbf{W}}_i^T \dot{\tilde{\mathbf{W}}}_i \\ &= -\sum_{i=1}^l \frac{k_1 k_{bi}^2}{\pi} \tan\left(\frac{\pi x_{1i}^2}{2k_{bi}^2}\right) - k_2 \mathbf{x}_2^T \mathbf{x}_2 + \mathbf{x}_2^T \boldsymbol{\varepsilon}(\mathbf{Z}) - \sum_{i=1}^l \eta_i \tilde{\mathbf{W}}_i^T \dot{\tilde{\mathbf{W}}}_i. \end{aligned} \quad (37)$$

The following inequalities can be easily derived:

$$-\tilde{\mathbf{W}}_i^T \dot{\tilde{\mathbf{W}}}_i = -\|\tilde{\mathbf{W}}_i\|^2 - \tilde{\mathbf{W}}_i^T \mathbf{W}_i^* \leq -\frac{1}{2} \|\tilde{\mathbf{W}}_i\|^2 + \frac{1}{2} \|\mathbf{W}_i^*\|^2, \quad (38)$$

$$\mathbf{x}_2^T \boldsymbol{\varepsilon}(\mathbf{Z}) \leq \frac{1}{2} \mathbf{x}_2^T \mathbf{x}_2 + \frac{1}{2} \bar{\varepsilon}^2. \quad (39)$$

Substituting (38) and (39) into (37), we further have

$$\begin{aligned} \dot{V}_3 &\leq -\sum_{i=1}^l \frac{k_1 k_{bi}^2}{\pi} \tan\left(\frac{\pi x_{1i}^2}{2k_{bi}^2}\right) - \left(k_2 - \frac{1}{2}\right) \mathbf{x}_2^T \mathbf{x}_2 - \frac{1}{2} \|\tilde{\mathbf{W}}_i\|^2 + \frac{1}{2} \|\mathbf{W}_i^*\|^2 + \frac{1}{2} \bar{\varepsilon}^2 \\ &\leq -\rho V_3 + \mathcal{G}, \end{aligned} \quad (40)$$

where ρ and \mathcal{G} are defined as

$$\rho = \min \left\{ k_1, \frac{2k_2 - 1}{\lambda_{\max}(\mathbf{H}(\mathbf{q}))}, \min_{i=1,2,\dots,l} \left\{ \frac{\eta_i}{\lambda_{\max}(\boldsymbol{\Gamma}_i^{-1})} \right\} \right\}, \quad (41)$$

$$\mathcal{G} = \frac{1}{2} \|\mathbf{W}_i^*\|^2 + \frac{1}{2} \bar{\varepsilon}^2. \quad (42)$$

Here, we must set $k_2 > 1/2$ to ensure $\rho > 0$. Then, solving (40), it follows that

$$V_3 \leq V_3(0) + \frac{\mathcal{G}}{\rho}. \quad (43)$$

This implies that the resulting closed-loop system is semiglobally uniformly ultimately bounded. Define the variable

$\mu = V_3(0) + \frac{\mathcal{G}}{\rho}$. Combining with the definition of V_3 , we can obtain

$$\frac{k_{bi}^2}{\pi} \tan\left(\frac{\pi x_{1i}^2}{2k_{bi}^2}\right) \leq \mu, \quad (44)$$

$$\mathbf{x}_2^T \mathbf{H}(\mathbf{q}) \mathbf{x}_2 \leq 2\mu, \quad (45)$$

$$\sum_{i=1}^l \tilde{\mathbf{W}}_i^T \boldsymbol{\Gamma}_i^{-1} \tilde{\mathbf{W}}_i \leq 2\mu. \quad (46)$$

Particularly, from (44), we further have

$$x_{1i}^2 \leq \frac{2k_{bi}^2}{\pi} \tan^{-1}\left(\frac{\pi\mu}{k_{bi}^2}\right) \leq \frac{2k_{bi}^2}{\pi} \frac{\pi}{2} = k_{bi}^2. \quad (47)$$

Thus, the error variables \mathbf{x}_1 , \mathbf{x}_2 , and $\tilde{\mathbf{W}}$ can eventually stabilize to the small residual sets $\boldsymbol{\Omega}_1$, $\boldsymbol{\Omega}_2$, and $\boldsymbol{\Omega}_3$ defined as (32)-(34), respectively. Moreover, from (47), we can obtain that the position tracking errors \mathbf{q}_e can never exceed the predefined output constraints $-\mathbf{k}_b(t) \leq \mathbf{q}_e(t) \leq \mathbf{k}_b(t)$ when the initial position of the space manipulator satisfies $-\mathbf{k}_b(0) \leq \mathbf{q}_e(0) \leq \mathbf{k}_b(0)$. The proof is finished. ■

3.3. Discussions

Remark 1. When the space manipulator does not suffer from output constraints, by L'Hospital's rule, the virtual stabilizer (22) becomes

$$\begin{aligned}
 \mathbf{a} = \lim_{k_{bl} \rightarrow +\infty} & \begin{bmatrix} -\frac{k_1 k_{b1}^2}{\pi x_{11}} \sin\left(\frac{\pi x_{11}^2}{2k_{b1}^2}\right) \cos\left(\frac{\pi x_{11}^2}{2k_{b1}^2}\right) - \frac{2k_{b1} \dot{k}_{b1}}{\pi x_{11}} \sin\left(\frac{\pi x_{11}^2}{2k_{b1}^2}\right) \cos\left(\frac{\pi x_{11}^2}{2k_{b1}^2}\right) + \left(\frac{\dot{k}_{b1}}{k_{b1}}\right) x_{11} \\ -\frac{k_1 k_{b2}^2}{\pi x_{12}} \sin\left(\frac{\pi x_{12}^2}{2k_{b2}^2}\right) \cos\left(\frac{\pi x_{12}^2}{2k_{b2}^2}\right) - \frac{2k_{b2} \dot{k}_{b2}}{\pi x_{12}} \sin\left(\frac{\pi x_{12}^2}{2k_{b2}^2}\right) \cos\left(\frac{\pi x_{12}^2}{2k_{b2}^2}\right) + \left(\frac{\dot{k}_{b2}}{k_{b2}}\right) x_{12} \\ \vdots \\ -\frac{k_1 k_{bl}^2}{\pi x_{1l}} \sin\left(\frac{\pi x_{1l}^2}{2k_{bl}^2}\right) \cos\left(\frac{\pi x_{1l}^2}{2k_{bl}^2}\right) - \frac{2k_{bl} \dot{k}_{bl}}{\pi x_{1l}} \sin\left(\frac{\pi x_{1l}^2}{2k_{bl}^2}\right) \cos\left(\frac{\pi x_{1l}^2}{2k_{bl}^2}\right) + \left(\frac{\dot{k}_{bl}}{k_{bl}}\right) x_{1l} \end{bmatrix} \\
 & = -k_1 \mathbf{x}_1.
 \end{aligned} \tag{48}$$

The unified neural controller (30) becomes

$$\begin{aligned}
 \boldsymbol{\tau}_c = \lim_{k_{bi} \rightarrow +\infty} & \begin{bmatrix} -\frac{x_{11}}{\cos^2\left(\frac{\pi x_{11}^2}{2k_{b1}^2}\right)} \\ -\frac{x_{12}}{\cos^2\left(\frac{\pi x_{12}^2}{2k_{b2}^2}\right)} \\ \vdots \\ -\frac{x_{1l}}{\cos^2\left(\frac{\pi x_{1l}^2}{2k_{bl}^2}\right)} \end{bmatrix} - k_2 \mathbf{x}_2 - \hat{\mathbf{W}}^T \boldsymbol{\Theta}(\mathbf{Z}) \\
 & = -\mathbf{x}_1 - k_2 \mathbf{x}_2 - \hat{\mathbf{W}}^T \boldsymbol{\Theta}(\mathbf{Z}).
 \end{aligned} \tag{49}$$

Moreover, the NN weight learning law (31) remains the same. Under this situation, the controller can still guarantee the semiglobal uniform ultimate boundedness of the resulting closed-loop system. By utilizing the tan-type BLF, the proposed controller can freely switched for the trajectory tracking of space manipulator no matter in the presence or absence of output constraints. Nevertheless, when the controllers are designed based on the log-type BLF (Yao, 2021a, 2021b), they are no longer applicable once the output constraints are removed. Therefore, a remarkable advantage of the proposed controller is that it is universal for the cases with and without considering the output constraints.

Remark 2. By utilizing the backstepping control technique as the main framework, the proposed controller is developed with the help of NN and tan-type BLF. To facilitate the readers for a better understanding, the structure of the proposed unified neural control scheme is presented in Fig. 2.

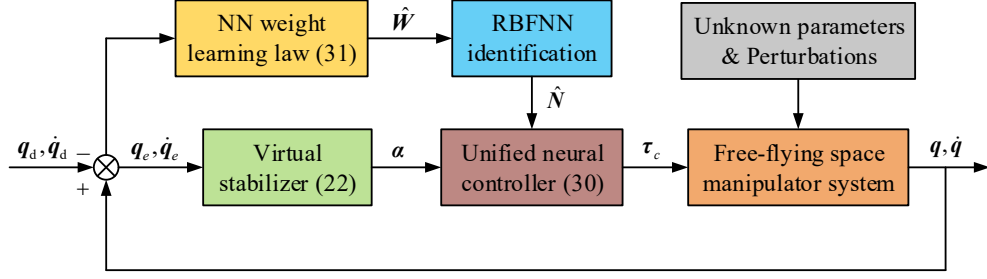


Fig. 2. Structure of the proposed unified neural control scheme.

Remark 3. By introducing the RBFNN to identify the unknown part in the dynamic model and then compensating it in the feedforward loop, the proposed controller is model-free and insensitive to external perturbations. Moreover, it should be pointed out that the RBFNN utilized in this work can also be replaced by some other identification tools, such as back propagation NN, wavelet NN, Chebyshev NN, and fuzzy logic systems.

4. Simulations and comparisons

4.1. Simulation scenario set up

In this section, simulations and comparisons are given to test the proposed unified neural control scheme. The simulation scenario is selected as a planar free-flying two-link space manipulator for non-cooperative target capturing as shown in Fig. 3. The detailed expressions for the dynamics of the two-link space manipulator can be found in Yao (2021a, 2021b, 2022).

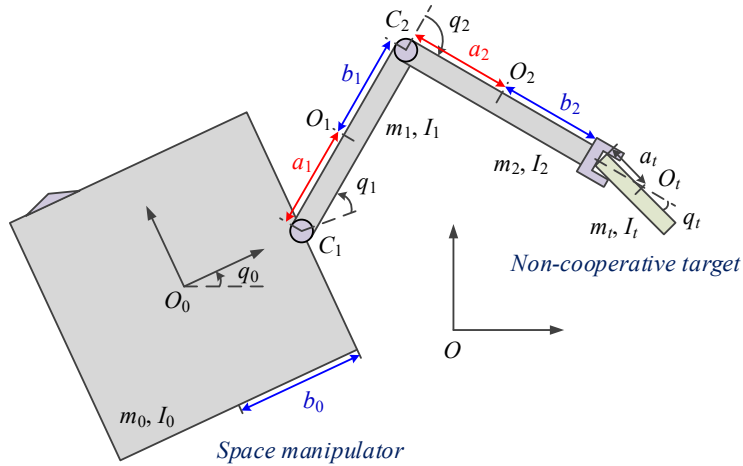


Fig. 3. Diagram of a two-link space manipulator for target capturing.

The physical and geometric parameters of the space manipulator are given as $m_0 = 60 \text{ kg}$, $m_1 = 6 \text{ kg}$, $m_2 = 5 \text{ kg}$, $m_t = 10 \text{ kg}$, $I_0 = 22.5 \text{ kg} \cdot \text{m}^2$, $I_1 = 1.125 \text{ kg} \cdot \text{m}^2$, $I_2 = 0.9375 \text{ kg} \cdot \text{m}^2$, $I_t = 2 \text{ kg} \cdot \text{m}^2$,

$b_0 = a_1 = b_1 = a_2 = b_2 = 0.75 \text{ m}$, $a_l = 0.5 \text{ m}$, $q_l = \pi/6 \text{ rad}$. All these parameters are assumed to be fully unknown in the control design. The external perturbations are chosen as $\delta = 0.1[\sin(0.4t), \cos(0.6t), \cos(0.4t)]^T \text{ Nm}$. The maximum acceptable control torque value is set as $\tau_m = 10 \text{ N}$. Moreover, the initial position and velocity of the space manipulator are chosen as $q(0) = [0.1, -0.2, 0.2]^T \text{ rad}$ and $\dot{q}(0) = [0.04, 0.02, -0.03]^T \text{ rad/s}$, respectively. The desired position is set as $q_d = [0, 0, 0]^T \text{ rad}$.

In what follows, two case studies with and without considering the output constraints are provided for simulations.

4.2. Case study considering the output constraints

In Case 1, the trajectory tracking control of space manipulator with output constraints is investigated. The output constraints are predefined as $k_{bi}(t) = 0.299e^{-0.2t} + 0.001$, $i = 1, 2, 3$. Besides the proposed unified neural controller, two existing controllers are also employed for comparisons. The first compared controller is the proportional-differential (PD) controller, which is designed as

$$\tau_c = -k_p q_e - k_d \dot{q}_e, \quad (50)$$

where $k_p > 0$ and $k_d > 0$. The second compared controller is the sliding mode controller. The sliding surface is constructed as

$$s = q_e + \sigma \dot{q}_e, \quad (51)$$

where $\sigma > 0$. Then, the sliding mode controller is designed as

$$\tau_c = -ks - h \operatorname{sgn}(s), \quad (52)$$

where $k > 0$ and $h > 0$. To attenuate chattering in the control design, the signum function $\operatorname{sgn}(s)$ can be replaced by the saturation function $\operatorname{sat}(s)$, whose elements are given as

$$\operatorname{sat}(s_i) = \begin{cases} \operatorname{sgn}(s_i), & |s_i| \geq \gamma, \\ s_i/\gamma, & |s_i| < \gamma, \end{cases} \quad i = 1, 2, \dots, l, \quad (53)$$

where γ is a small positive constant. A common feature of the proposed controller and two compared controllers is that they are all model-free.

The design parameters of the proposed unified neural controller (30) are selected as $k_1 = 1$, $k_2 = 40$, $\Gamma_i = 200\mathbf{I}_7$, and $\eta_i = 0.01$. Seven neurons are set for each RBFNN. The center of $\theta_i(Z)$ is selected as $\Psi_i = [-3, -2, -1, 0, 1, 2, 3]^T$ and the width is set as $b_i = 6$. The initial values of the RBFNN weight identifications are set as $\hat{W}_i(0) = \mathbf{0}_7$. In addition, the design parameters of the PD controller (50) are selected as $k_p = 100$ and $k_d = 80$. The design parameters of the sliding mode controller (52) are selected as $\sigma = 1$, $k = 80$, $h = 0.01$ and $\gamma = 0.01$.

The simulation results for Case 1 are presented in Figs. 4-7. Figs. 4 and 5 show the curves of the position tracking and velocity tracking, respectively. It is clearly seen that the space manipulator can fulfill the trajectory tracking under the proposed and compared controllers. The position and velocity steady-state tracking errors under the proposed controller are within the ranges of $[-4 \times 10^{-4}, 4 \times 10^{-4}]^T$ rad and $[-2 \times 10^{-4}, 2 \times 10^{-4}]^T$ rad/s, respectively. By contrast, the position and velocity steady-state tracking errors under two compared controllers are within the ranges of $[-3 \times 10^{-3}, 3 \times 10^{-3}]^T$ rad and $[-2 \times 10^{-3}, 2 \times 10^{-3}]^T$ rad/s, respectively. Therefore, the proposed controller can achieve the more excellent tracking performance than the PD controller and the sliding mode controller in terms of higher steady-state tracking accuracy. The simulation results are well consistent with the theoretical analysis in Section 4. Benefiting from neural identification, which makes the proposed controller model-free and insensitive to external perturbations.

Moreover, from Fig. 4, the position tracking errors under two compared controllers obviously exceed the upper and lower bounds. Alternatively, the proposed controller can preserve the position tracking errors always within the predefined output constraints. This is mainly owing to the adaption of tan-type BLF, based on which the proposed controller has the capability to handle the output constraints.

Additionally, the curves of the control torques are given in Fig. 6. The control torques under the proposed and compared controllers satisfy the actuator saturation constraints. Fig. 7 provides the norms of the NN weight identifications. The NN weight is online learned and can change with time smoothly.

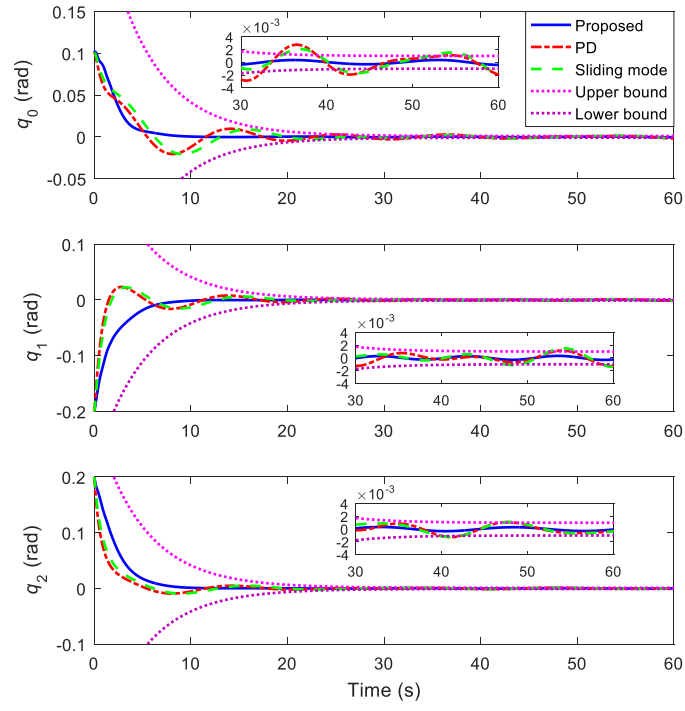


Fig. 4. Curves of the position tracking (Case 1).

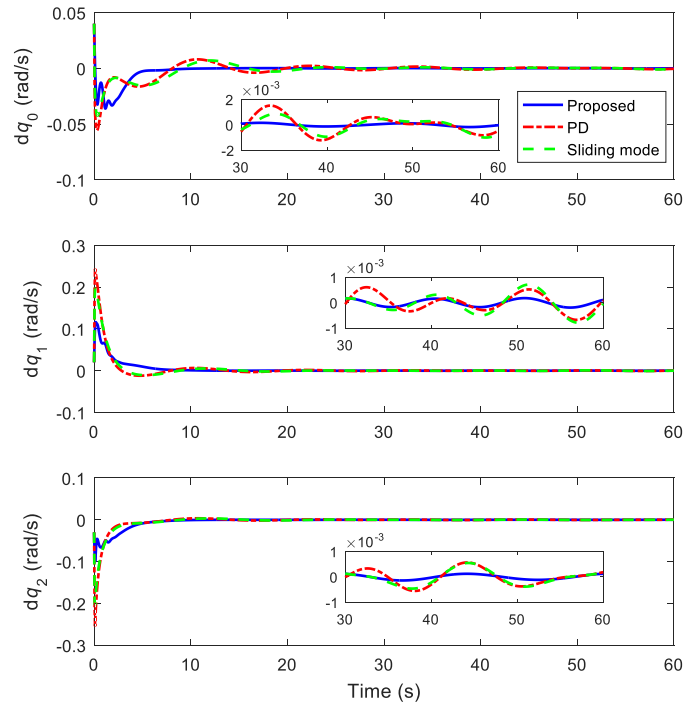


Fig. 5. Curves of the velocity tracking (Case 1).

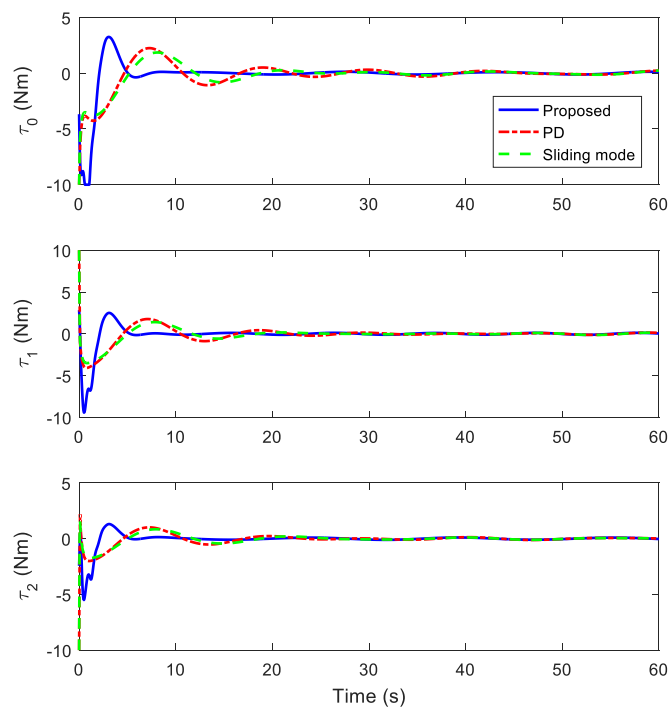


Fig. 6. Curves of the control torques (Case 1).

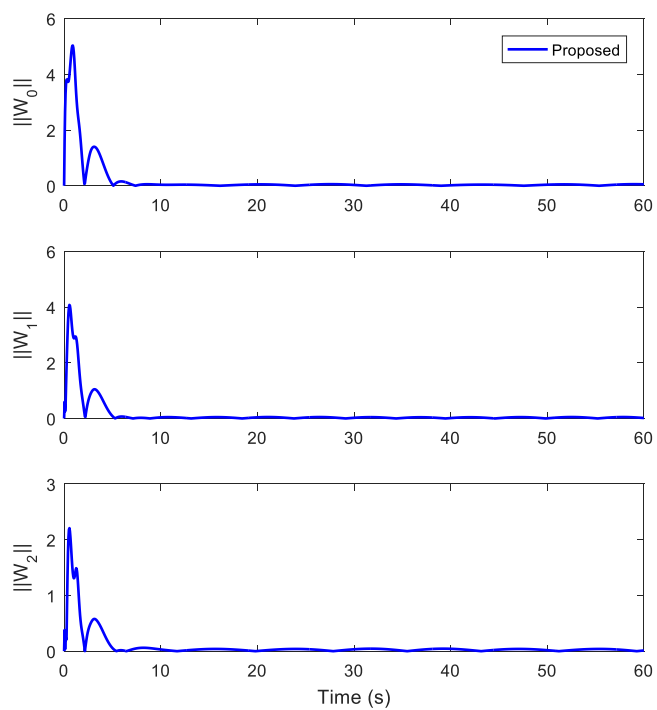


Fig. 7. Norms of the NN weight identifications (Case 1).

4.3. Case study without considering the output constraints

In Case 2, the trajectory tracking control of space manipulator without output constraints is addressed. All simulation conditions are set the same as those in Case 1. The proposed controller is utilized for simulations and the design parameters are also selected the same as those in Case 1.

The simulation results for Case 2 are shown in Figs. 8-11. It is not difficult to find that the excellent tracking performance can still be achieved under the proposed controller. Combining the simulation results of Cases 1 and 2, the proposed controller can realize the high-performance trajectory tracking of space manipulator no matter in the presence or absence of output constraints. Consequently, we can conclude that the proposed controller universal for the cases with and without considering the output constraints. As mentioned in Remark 1, this is a remarkable advantage of the proposed controller by the aid of tan-type BLF. By contrast, the log-type BLF-based controllers in Yao (2021a, 2021b) cannot be utilized when the space manipulator does not suffer from output constraints.

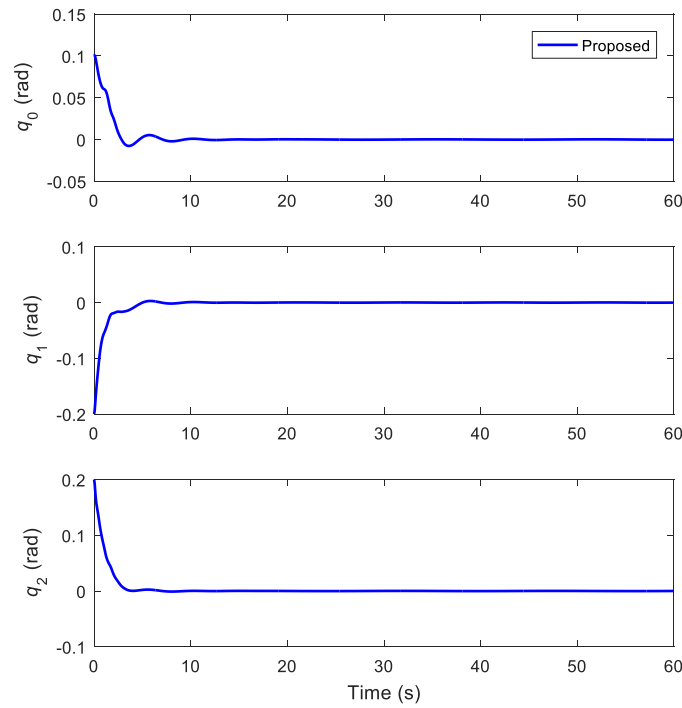


Fig. 8. Curves of the position tracking (Case 2).

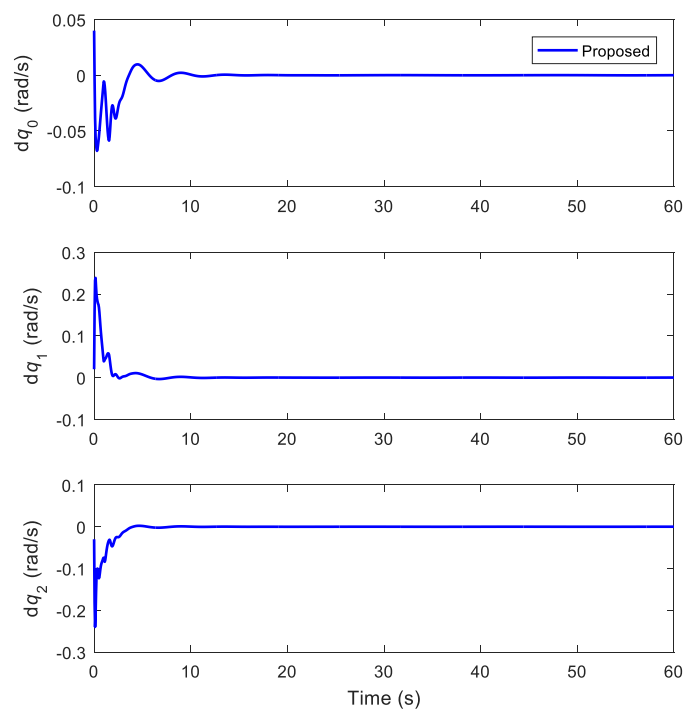


Fig. 9. Curves of the velocity tracking (Case 2).

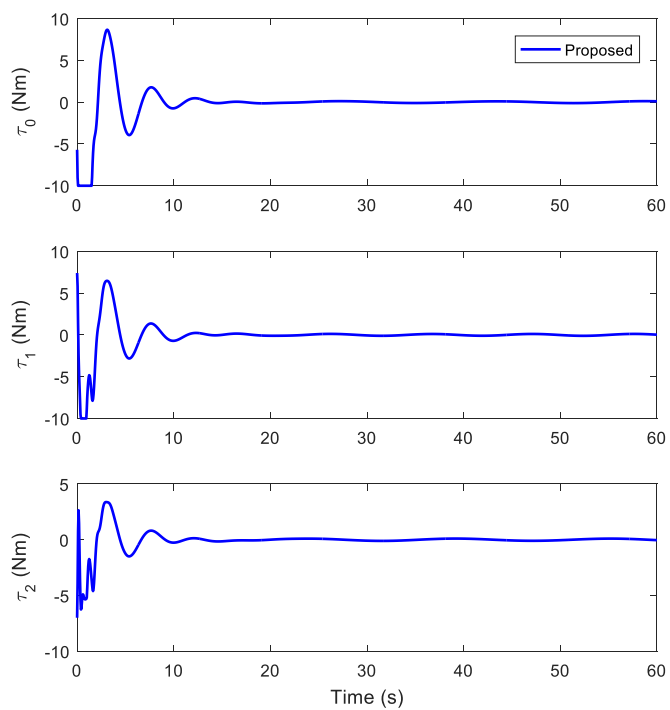


Fig. 10. Curves of the control torques (Case 2).

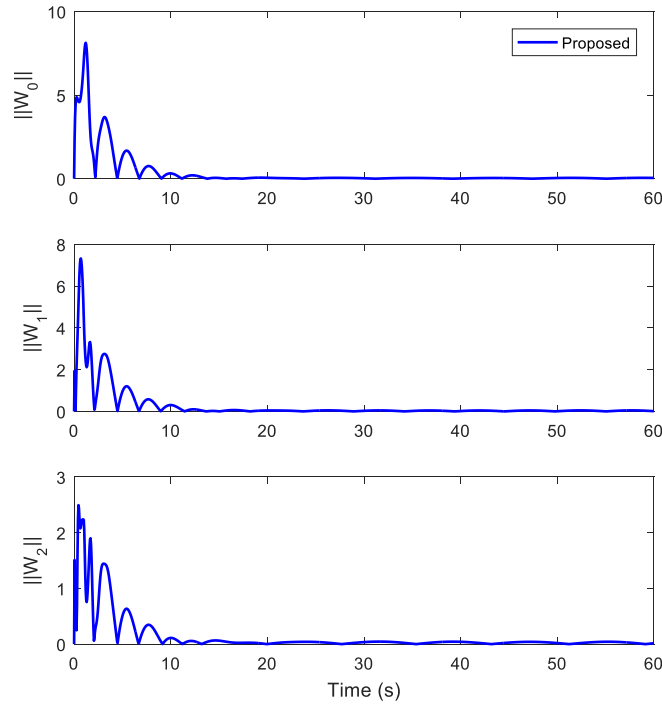


Fig. 11. Norms of the NN weight identifications (Case 2).

5. Conclusions

This paper addresses the challenging problem of the trajectory tracking of unknown space manipulator under output constraints. A unified neural control scheme is originally proposed by combining NN and tan-type BLF under the framework of backstepping control technique. On the one hand, the proposed controller is model-free and insensitive to external perturbations by the aid of neural identification. On the other hand, the proposed controller can preserve the position tracking errors always within the predefined output constraints by utilizing the tan-type BLF. Moreover, it should be emphasized that rather than log-type BLF-based controllers, the proposed controller is universal for the cases with and without considering the output constraints. Strict stability argument shows that the resulting closed-loop system is semiglobally uniformly ultimately bounded under the proposed controller. Lastly, a planar free-flying two-link space manipulator for non-cooperative target capturing is utilized for simulation studies. The simulation results indicate that the proposed controller is effective and can achieve the more excellent tracking performance than two existing controllers. For the future research of this work, we will attempt to extend the proposed unified neural control scheme with the finite-time or fixed-time convergence capability.

384

385 **References**

- 386 Chu, Z., Cui, J., Sun, F., 2014. Fuzzy adaptive disturbance-observer-based robust tracking control of electrically
387 driven free-floating space manipulators. *IEEE Syst. J.* 8 (2), 343-352.
- 388 Chu, Z., Li, J., Lu, S., 2015. The composite hierarchical control of multi-link multi-DOF space manipulator based on
389 UDE and improved sliding mode control. *Proc. Inst. Mech. Eng., Part G: J. Aerosp. Eng.* 229 (14), 2646-2658.
- 390 Flores-Abad, A., Ma, O., Pham, K., Ulrich, S., 2014. A review of space robotics technologies for on-orbit serving.
391 *Prog. Aerosp. Sci.* 68, 1-26.
- 392 Jayakody, H.S., Katupitiya, J., Kinkaid, N., 2016. Robust adaptive coordination controller for a spacecraft equipped
393 with a robotic manipulator. *J. Guid. Control Dyn.* 39 (12), 2699-2711.
- 394 Jia, S., Jia, Y., Xu, S., Hu, Q., 2018. Maneuver and active vibration suppression of free-flying space robot. *IEEE*
395 *Trans. Aerosp. Electron. Syst.* 54 (3), 1115-1134.
- 396 Jia, S., Shan, J., 2020. Finite-time trajectory tracking control of space manipulator under actuator saturation. *IEEE*
397 *Trans. Ind. Electron.* 67 (3), 2086-2096.
- 398 Jia, Q., Yuan, B., Chen, G., Fu, Y., 2021. Adaptive fuzzy terminal sliding mode control for the free-floating space
399 manipulator with free-swinging joint failure. *Chin. J. Aeronaut.* 34 (9), 178-198.
- 400 Jin, R., Rocco, P., Geng, Y., 2021. Observer-based fixed-time tracking control for space robots in task space. *Acta*
401 *Astronaut.* 184, 35-45.
- 402 Jin, X., Xu, J.-X., 2013. Iterative learning control for output-constrained systems with both parametric and
403 nonparametric uncertainties. *Automatica* 49 (8), 2508-2516.
- 404 Kumar, N., Panwar, V., Borm, J.-H., Chai, J., Yoon, J., 2013. Adaptive neural controller for space robot system with
405 an attitude controlled base. *Neural Comput. Appl.* 23 (7-8), 2333-2340.
- 406 Li, W.-J., Cheng, D.-Y., Liu, X.-G., Wang, Y.-B., Shi, W.-H., Tang, Z.-X., Gao, F., Zeng, F.-M., Chai, H.-Y., Luo,
407 W.-B., Cong, Q., Gao, Z.-L., 2019. On-orbit service (OOS) of spacecraft: A review of engineering developments.
408 *Prog. Aerosp. Sci.* 108, 32-120.
- 409 Moghaddam, B.M., Chhabra, R., 2021. On the guidance, navigation and control of in-orbit space robotic missions:
410 A survey and prospective vision. *Acta Astronaut.* 184, 70-100.

- Moosavian, S.A.A., Papadopoulos, E., 2007. Free-flying robots in space: an overview of dynamics modeling, planning and control. *Robotica* 25 (5), 537-547.
- Nekoo, S.R., 2019. Model reference adaptive state-dependent Riccati equation control of nonlinear uncertain systems: Regulation and tracking of free-floating space manipulators. *Aerosp. Sci. Technol.* 84, 348-360.
- Parlaktuna, O., Ozkan, M., 2004. Adaptive control of free-floating space manipulators using dynamically equivalent manipulator model. *Robot. Auton. Syst.* 46 (3), 185-193.
- Pazelli, T.F.P.A.T., Terra, M.H., Siqueira, A.A.G., 2011. Experimental investigation on adaptive robust controller designs applied to a free-floating space manipulator. *Control Eng. Pract.* 19 (4), 395-408.
- Qin, L., Liu, F., Liang, L., Gao, J., 2014. Fuzzy adaptive robust control for space robot considering the effect of the gravity. *Chin. J. Aeronaut.* 27 (6), 1562-1570.
- Ren, B., Ge, S.S., Tee, K.P., Lee, T.H., 2010. Adaptive neural control for output feedback nonlinear systems using a barrier Lyapunov function. *IEEE Trans. Neural Netw.* 21 (8), 1339-1345.
- Rybus, T., Seweryn, K., Sasiadek, J.Z., 2017. Control system for free-floating space manipulator based on nonlinear model predictive control (NMPC). *J. Intell. Robot. Syst.* 85 (3-4), 491-509.
- Sanner, R.M., Slotine, J.-J.E., 1992. Gaussian networks for direct adaptive control. *IEEE Trans. Neural Netw.* 3 (6), 837-863.
- Seddaoul, A., Saaj, C.M., 2019. Combined nonlinear H_∞ controller for a controlled-floating space robot. *J. Guid. Control Dyn.* 42 (8), 1878-1885.
- Shao, X., Sun, G., Xue, C., Li, X., 2021. Nonsingular terminal sliding mode control for free-floating space manipulator with disturbance. *Acta Astronaut.* 181, 396-404.
- Shi, L., Kayastha, S., Katupitiya, J., 2017. Robust coordinated control of a dual-arm space robot. *Acta Astronaut.* 138, 475-489.
- Spong, M.W., Hutchinson, S., Vidyasagar, M., 2006. Robot modeling and control. John Wiley and Sons, New York.
- Tee, K.P., Ge, S.S., Tay, E.H., 2009. Barrier Lyapunov functions for the control of output-constrained nonlinear systems. *Automatica* 45 (4), 918-927.
- Tee, K.P., Ren, B., Ge, S.S., 2011. Control of nonlinear systems with time-varying output constraints. *Automatica* 47 (11), 2511-2516.

- Wang, H., 2011. On adaptive inverse dynamics for free-floating space manipulators. *Robot. Auton. Syst.* 59 (10), 782-788.
- Wang, H., Xie, Y., 2009a. Adaptive Jacobian position/force tracking control of free-flying manipulators. *Robot. Auton. Syst.* 57 (2), 173-181.
- Wang, H., Xie, Y., 2009b. Passivity based adaptive Jacobian tracking for free-floating space manipulators without using spacecraft acceleration. *Automatica* 45 (6), 1510-1517.
- Wang, H., Xie, Y., 2012. Prediction error based adaptive Jacobian tracking of free-floating space manipulators. *IEEE Trans. Aerosp. Electron. Syst.* 48 (4), 3207-3221.
- Xu, J.-X., Jin, X., 2013. State-constrained iterative learning control for a class of MIMO systems. *IEEE Trans. Autom. Control* 58 (5), 1322-1327.
- Yang, H., Yu, Y., Yuan, Y., Fan, X., 2015. Back-stepping control of two-link flexible manipulator based on an extended state observer. *Adv. Space Res.* 56 (10), 2312-2322.
- Yao, Q., 2021a. Adaptive trajectory tracking control of a free-flying space manipulator with guaranteed prescribed performance and actuator saturation, *Acta Astronaut.* 185, 283-298.
- Yao, Q., 2021b. Adaptive fuzzy neural network control for a space manipulator in the presence of output constraints and input nonlinearities, *Adv. Space Res.* 67 (6), 1830-1843.
- Yao, Q., 2022. Robust finite-time trajectory tracking control for a space manipulator with parametric uncertainties and external disturbances. *Proc. Inst. Mech. Eng., Part G: J. Aerosp. Eng.* 236 (2), 396-409.
- Yu, X., Chen, L., 2015. Modeling and observer-based augmented adaptive control of flexible-joint free-floating space manipulators, *Acta Astronaut.* 108, 146-155.
- Zhan, B., Jin, M., Liu, J., 2022. Extended-state-observer-based adaptive control of flexible-joint space manipulators with system uncertainties, *Adv. Space Res.* 69 (8), 3088-3102.
- Zhang, S., Li, C., Zheng, J., Wang, X., Zeng, Z., Chen, G., 2021b. Generating any number of diversified hidden attractors via memristor coupling. *IEEE Trans. Circuits Syst. I: Reg. Papers* 68 (12), 4945-4956.
- Zhang, S., Li, C., Zheng, J., Wang, X., Zeng, Z., Peng, X., 2022. Generating any number of initial offset-boosted coexisting Chua's double-scroll attractors via piecewise-nonlinear memristor. *IEEE Trans. Ind. Electron.* 69 (7), 7202-7212.

- 465 Zhang, W., Ye, X., Jiang, L., Zhu, Y., Ji, X., Hu, X., 2013. Output feedback control for free-floating space robotic
466 manipulators base on adaptive fuzzy neural network. *Aerosp. Sci. Technol.* 29 (1), 135-143.
- 467 Zhang, S., Zheng, J., Wang, X., Zeng, Z., Peng, X., 2021a. A novel nonideal flux-controlled memristor model for
468 generating arbitrary multi-double-scroll and multi-double-wing attractors. *Int. J. Bifurcation Chaos* 31 (6), 2150086.
- 469 Zhou, Z.-G., Zhang, Y.-A., Zhou, D., 2017. Robust prescribed performance tracking control for free-floating space
470 manipulators with kinematic and dynamic uncertainty. *Aerosp. Sci Technol.* 71, 568-579.
- 471 Zhu, Y., Qiao, J., Guo, L., 2019. Adaptive sliding mode disturbance observer-based composite control with
472 prescribed performance of space manipulators for target capturing. *IEEE Trans. Ind. Electron.* 66 (3), 1973-1983.